Article | Received 16 June 2023; Accepted 28 September 2023; Published 27 October 2023
https://doi.org/10.55092/exrna20230007

Exploration of neuroblastoma xenograft models for tumor extracellular RNA profiling in murine blood plasma

Jill Deleu[1,2,†], Hanne Van Droogenbroeck[1,2,†], Jasper Anckaert[1,2], Anneleen Decock[1,2], Jilke De Wilde[2,3], Kaat Durinck[2,4], Liselot M. Mus[2,4,5], Justine Nuytens[1,2], Muhammad Rishfi[2,4], Kathleen Schoofs[1,2,6], Frank Speleman[2,4], Maaike Van Trimpont[2,7,8], Kimberly Verniers[1,2], Nurten Yigit[1,2], Jo Vandesompele[1,2,*], Bram De Wilde[1,2,4,5,9,‡] and Tom Van Maerken[1,2,10,‡]

[1] OncoRNALab, Cancer Research Institute Ghent (CRIG), Ghent, Belgium
[2] Department of Biomolecular Medicine, Ghent University, Ghent, Belgium
[3] Department of Pathology, Ghent University Hospital, Ghent, Belgium
[4] Pediatric Precision Oncology Lab (PPOL), Cancer Research Institute Ghent (CRIG), Ghent, Belgium
[5] Department of Paediatric Haematology Oncology and Stem Cell Transplantation, Ghent University Hospital, Ghent, Belgium
[6] TOBI lab, VIB – Ghent University, Zwijnaarde, Belgium
[7] Department of Diagnostic Sciences, Ghent University, Ghent, Belgium
[8] Lab Normal and Malignant Hematopoiesis, Cancer Research Institute Ghent (CRIG), Ghent, Belgium
[9] Department of Internal Medicine and Pediatrics, Ghent University, Ghent, Belgium
[10] Department of Laboratory Medicine, AZ Groeninge, Kortrijk, Belgium
† They are joint first authors and contributed equally to this work.
‡ They are joint last authors and contributed equally to this work.

* Correspondence author; E-mail: jo.vandesompele@ugent.be.

Abstract: Background: Minimally invasive liquid biopsies are becoming increasingly important in the diagnosis and treatment follow-up of cancer patients, including children with neuroblastoma. Such biopsies contain various biomarker analytes, including extracellular RNA (exRNA) with the potential to reflect dynamic changes in the tumor. However, it is challenging to distinguish tumor-derived exRNA from normal RNA. To overcome this limitation, xenograft models serve as a practical tool. In a mouse engrafted with human tumor cells, human exRNA is by definition originating from the tumor, whereas murine exRNA is host-derived. To study treatment response by monitoring tumor-derived exRNA, xenograft models with a high release of tumor exRNA into the circulation are desirable. Methods: The aim of this study was to evaluate whether and to what extent the cell line, its engraftment

site, or the tumor size influence the amount of tumoral exRNA detected in blood plasma. To that end, four different neuroblastoma cell lines were engrafted in nude mice, either subcutaneously in the flank or orthotopically in the adrenal gland. Tumor sizes were monitored by caliper measurements (subcutaneous grafts) or MRI scans (orthotopic grafts) and blood was collected via terminal cardiac puncture to evaluate the tumoral exRNA fraction. Results: We demonstrate that the tumoral exRNA levels are correlated with the size of the subcutaneous tumor grafts. These levels are also highly dependent on the engrafted cell line. Furthermore, orthotopic engraftment potentially results in superior levels of tumoral exRNA, likely because of higher vascularity of the tumor tissue. Conclusions: Factors as cell line, tumor size and injections site should carefully be considered when performing experiments to study circulating RNA biomarkers.

Keywords: liquid biopsies; extracellular RNA; cell-free RNA; murine xenografts; neuroblastoma

1. Introduction

Neuroblastoma is the most frequent extracranial childhood tumor, accounting for up to 15% of pediatric oncology deaths [1]. It presents with a broad clinical behavior ranging from an asymptomatic benign malignancy with spontaneous regression to very aggressively proliferative tumors that are widely disseminated and often fatal [2]. High-risk neuroblastoma (HR-NB) patients are treated with intensive multimodal therapies, consisting of induction chemotherapy, surgery to remove the primary tumor, consolidation with high-dose chemotherapy followed by autologous stem cell transplantation, radiotherapy to the site of the primary tumor and maintenance therapy consisting of anti-GD2 immunotherapy and 13-cis-retinoic acid [3,4]. Despite these intensive multimodal therapies, half of HR-NB patients still show relapsed or refractory disease, due to treatment-resistant minimal residual disease (MRD) [3]. Additionally, small tissue biopsies may not represent the entire tumor, because of intratumor heterogeneity [5]. Furthermore, such spatial heterogeneity may lead to acquired resistance to therapy [6]. Performing sequential tissue biopsies to follow-up on therapeutic tumor responses is not feasible due to its invasiveness, the need for sedation, and tumors often not being accessible [7]. Detecting (chemo)resistant MRD at the earliest possible stage is key to improving the outcome of HR-NB patients by initiating targeted treatments early on [8]. Hence, liquid biopsies such as blood plasma, have emerged as a novel, minimally invasive opportunity of detecting and monitoring neuroblastoma in biofluids instead of tumor tissue [5].

Several studies have indicated the presence of circulating tumor DNA (ctDNA) in the blood plasma of neuroblastoma patients. Targetable single nucleotide variants (SNVs, e.g., ALK mutations) and copy number alterations (CNAs, e.g., MYCN amplification and ALK amplification) are detectable in ctDNA by digital PCR and (shallow) whole genome sequencing [7,9–15]. Moreover, some SNVs are only detected in the ctDNA and not in the tissue biopsy, reflecting the spatial heterogeneity of neuroblastoma tumors. In contrast, CNAs are similar between ctDNA and primary tissue, suggesting that the spatial heterogeneity is minimal for CNAs [7,8,15]. Furthermore, it has been demonstrated that the

(tumor-derived) cell-free DNA (cfDNA) levels are higher in HR-NB patients compared to healthy controls, and in metastatic *versus* localized disease [8,14,16]. Therefore, capturing CNAs and SNVs was only successful in a minority of low stage localized tumors [8,10,14,16]. ExRNA may be able to overcome this challenge due to its wide dynamic range. In addition, while DNA is the static blueprint for cellular processes, RNA is produced on demand when specific processes are needed and is therefore – in principle - more suited to evaluate treatment responses. exRNA includes a variety of RNA types, e.g., microRNA, long non-coding RNA, messenger RNA, circular RNA, piwi-interacting RNA, and transfer RNA (fragments), all of which have been identified in various biofluids [17,18]. To protect exRNA from degradation, they are encapsulated in extracellular vesicles or lipid nanoparticles, or they bind to proteins [19]. Except for microRNAs, all types of RNA are present in our dataset (because of the specific library prep method), with the majority being messenger RNA [20]. To explore the value of exRNA, we have developed neuroblastoma cell line derived xenograft models, *i.e.*, mouse models engrafted with human tumor cells. In our previous work, we developed a computational pipeline to distinguish human (tumor) from murine (host) sequencing reads in fragmented and low abundant exRNA present in murine plasma [20]. In addition, we put forward platelet-depleted plasma to study therapeutic responses as host background exRNA levels increased with increasing platelet levels and showed that the detectability of tumor transcripts in plasma exRNA is associated with the abundance levels in the tissue of neuroblastoma and breast cancer xenograft models [20]. Here, we evaluate the influence of the engrafted cell line, the engraftment site, and the tumor size on the tumoral exRNA levels in murine blood plasma. To exclude biases caused by tumor heterogeneity, we opted to use cell line derived xenograft models, as patient-derived xenograft models have shown to be associated with a higher degree of tumor heterogeneity [21].

We present this article in accordance with the ARRIVE checklist.

2. Methods

2.1. Tumor tissue and plasma collection

Experiments were performed under a project license (NO.: P164/2019, ECD 18-58, ECD 18-74, ECD 20-55 and ECD 20-63) granted by institutional ethics committees of KU Leuven and UGent in compliance with the universities' (KU Leuven and UGent) national or institutional guidelines for the care and use of animals. Two mouse cohorts were investigated: a first cohort to evaluate the influence of tumor size and the engrafted cell line on the exRNA amount (referred to as cell line cohort (n = 45, Table 1)) and a second cohort to evaluate the influence of the engraftment site on the exRNA amount (referred to as engraftment site cohort (n = 37, Table 1)). Mice were engrafted with four different neuroblastoma cell lines: IMR-32, NGP, SK-N-AS and SK-N-BE(2C). Plasma from mice in the cell line cohort was obtained as residual material from other studies, meaning that the selection of these cell lines was opportunistic. Of note, IMR-32, NGP, SK-N-AS and, SK-N-BE(2C) are commonly used neuroblastoma cell lines in the field of neuroblastoma research [22]. In addition, our laboratory has a track record of using these cell lines and has demonstrated the ability to

successfully establish murine xenografts, which is not possible with all neuroblastoma cell lines [23,24]. Supplemental Table S1 shows the characteristics and genetic profile of each of the cell lines used. STR genotyping has been performed before engraftment to confirm cell identity.

Table 1. Overview of mouse xenograft cohorts.

Number of mice	Cell line (number of cells)	Engraftment site (age)	Treatment	Tumor size at sacrifice (mm^3) (range and median)	Plasma preparation protocol	Mouse strain	Housing
Cell line cohort (female, n = 45)							
10	SK-N-AS (2.00×10^6)	subcutaneous (5 weeks)	vehicle	779–2871 (2262)	2-spin	crl:nu-foxn1^{nu}	Ghent University
13	IMR-32 (2.00×10^6)	subcutaneous (5-6 weeks)	vehicle	1949–2617 (2149)	2-spin (n = 6) 3-spin (n = 7)	crl:nu-foxn1^{nu}	Ghent University
7	IMR-32 (2.41×10^6)	subcutaneous (6 weeks)	vehicle	0–3323 (1949)	2-spin	BALB/c nude J no. 633	Ghent University
7	NGP (2.30×10^6)	subcutaneous (6 weeks)	vehicle	34–2564 (786)	2-spin	BALB/c nude J no. 633	Ghent University
8	SK-N-BE(2C) (2.00×10^6)	subcutaneous (13 weeks)	-	1166–2243 (2096)	3-spin	NMRI-foxn1^{nu}	KU Leuven
Engraftment site cohort (female, n = 37)							
9	SK-N-BE(2C) (1.00×10^6)	orthotopic (5-6 weeks)	-	no data	2-spin	BALB/c nude J no. 633	Ghent University
10	SK-N-BE(2C) (2.20×10^6)	subcutaneous (5-6 weeks)	-	807–3352 (2126)	2-spin		
8	IMR-32 (1.00×10^6)	orthotopic (5-6 weeks)	-	175–3215 (1698)	2-spin		
10	IMR-32 (3.00×10^6)	subcutaneous (5-6 weeks)	-	1879–2789 (2071)	2-spin		
82 in total							

Sample sizes were determined according to the sample size guidelines for mice experiments of Donna Neuberg [25]. A single animal is considered as the experimental unit in both cohorts. Female nude immunodeficient mice were used as it is easier to perform surgery (no shaving required), they are less aggressive, and have a larger adrenal gland compared to male mice [26,27]. A non-engrafted control group was not included as we only investigated the differences in exRNA levels between the models. The pipeline used to distinguish human (tumoral) and murine (host) reads was previously optimized using non-engrafted mice as a control [20]. Since the mice included in the cell line cohort were obtained as residual material from other experiments, different immunodeficient strains were included in this cohort: NMRI-Foxn1nu strain (IMSR_TAC:NMRINU; Taconic Biosciences, Rensselaer, NY, US), crl:nu-foxn1nu (RRID:IMSR_CRL:088; Charles River laboratories, Les Oncins, France) and BALB/c nude J no. 633 (RRID:IMSR_JAX:001026 Charles River Laboratories). Part of our analyses was performed on publicly available sequencing data that was previously generated (*i.e.*, 3-spin plasma from IMR-32 grafts and SK-N-BE(2C) grafts in the cell line cohort, Table 1) [20]. Of note, only mice that were administered with a vehicle control or did not receive any treatment, were included in this study. Four to five mice were housed per cage, and nesting material was provided for enrichment. Before any intervention, mice acclimatized for one week.

To establish subcutaneous, heterotopic models, a predefined number of cancer cells in 30 µl RPMI 1640 medium (Thermo Fisher Scientific, Waltham, MA, USA), suspended in 70 µl Matrigel matrix (Corning, Bedford, MA, UK), were engrafted in the dorsal flank (Table 1). Follow-up of tumor volume was performed two to three times per week by caliper measurements ($V = 0.5 \times a \times b \times b$, with a the longest side of the tumor and b the shortest side of the tumor). To establish orthotopic models, mice were anesthetized with isoflurane 4% and anesthesia was maintained with 2.6–2.7% isoflurane and 270 mL/min O_2, while keeping the mice on a heating plate to maintain body temperature. Buprenorphine (100 µl of an 11.4 µg/mL solution) was administered subcutaneously prior to the start of the surgery. After disinfection of the skin with chlorhexidine, an incision was made in the left flank at the level of the spleen. Subsequently, the neuroblastoma cell suspension (Table 1) was engrafted into the adrenal gland directed towards the kidney, as the adrenal gland became visible by carefully moving the spleen aside. The cell suspension was prepared upfront by suspending a predefined number of cells in 9 µl medium and 21 µl of Matrigel. The syringes, containing 30 µl of the suspension, were kept on 4 ℃ until engraftment, preventing the Matrigel to polymerize. Successful engraftment was confirmed by a visible swelling of the adrenal gland. After engraftment, the muscle layer was sutured with a coated vicryl suture 5-0 (polyglactin 910, C3 13mm 3/8c) and the skin was glued with Vetbond (3M). After surgery, mice were closely monitored for clinical signs of pain or distress. MRI scans were performed to follow up on the tumor size in the IMR-32 orthotopic mouse model. All mice were also weighed two to three times per week. After a predefined timeframe, or when mice reached specific humane endpoints (*i.e.*, a weight loss of more than 20% or clinical signs of significant pain, distress, or suffering), cardiac puncture was performed under isoflurane anesthesia, to collect blood, followed by cervical dislocation of the mice. The blood, collected in Microvette 500 K3EDTA tubes (Sarstedt, Newton, NC, USA), was processed immediately to prepare platelet-depleted plasma within two hours after cardiac puncture. The platelet-depleted plasma was prepared either by a 2-spin protocol (2 times 1900 g for 10 minutes) or a 3-spin protocol (400 g for 20 minutes, 800 g for 10 minutes and 2500 g for 15 minutes). In the engraftment site cohort, a part of the tumor was snap frozen and subjected to formalin-fixed paraffin embedding (FFPE) for histological analysis. The degree of hemolysis of plasma samples was assessed by measuring levels of hemoglobin by spectrophotometric analysis (OD414) using a NanoDrop 1000 spectrophotometer (Thermo Fisher Scientific; Supplemental Table S2). Engraftment, follow-up and euthanasia were performed by the same unblinded investigators to minimize experimental bias.

2.2. Hematoxylin and eosin staining of tumor tissue

Tissues were fixed in 10% neutral-buffered formalin and after 24 hours embedded in paraffin. Hematoxylin and eosin (H&E) staining was performed on 2–4 µm sections for morphological analysis. The mitotic count was obtained by counting the number of mitotic figures per 10 high-power fields (1 HPF = 0.26 mm^2). The tumor sections were ranked based on the average microvascular density (with 0 = no vessels and 5 = highest density) by a blinded pathologist.

2.3. RNA isolation, spike-in RNA addition and gDNA removal

ExRNA from 60 µl to 200 µl platelet-depleted plasma was isolated using the miRNeasy Serum/Plasma Kit (Qiagen, Hilden, Germany), according to the manufacturer's manual. During RNA extraction, 2 µl per 200 µl of plasma of a 3000-fold or 30,000-fold dilution of Sequin spike-in controls (Garvan Institute of Medical Research, Darlinghurst, NSW, Australia [28]) was added to the lysate. Upon RNA purification, 2 µl of a 25,000-fold, 50,000-fold or 70,000-fold dilution of External RNA Control Consortium (ERCC) RNA Spike-in Mix (Thermo Fisher Scientific) was added to 12 µl RNA eluate, followed by gDNA removal [29]. To remove residual DNA, 1 µl HL-dsDNase (ArcticZymes Technologies, Tromsø, Norway) and 1.4 µl Heat & Run 10X Reaction Buffer (ArcticZymes Technologies) were added to the eluates, and RNA samples were incubated for 10 min at 37 ℃, followed by 5 min at 58 ℃. An overview of the plasma input volumes and the amount of Sequin and ERCC spike-in controls added is shown in Supplemental Table S2.

2.4. Total RNA library preparation and sequencing

Total RNA libraries were prepared starting from 8 µl DNase-treated RNA using the SMARTer Stranded Total RNA-Seq Kit v2-Pico Input Mammalian (Takara Bio, CA, USA), according to the manufacturer's manual with minor modifications [30]. Briefly, prior to first strand cDNA synthesis, RNA was fragmented for 2 min at 94 ℃. During final library amplification, 16 PCR cycles were performed on the liquid biopsy samples. Final clean-up was repeated if an excessive number of products < 200 bp in size was observed on FragmentAnalyzer data (data not shown, Agilent Technologies, Santa Clara, CA, USA). Fragment sizes were determined using FragmentAnalyzer software for smear analysis in the 200 bp to 1000 bp range. Library quantification was performed using the KAPA Library quantification Kit (Kapa Biosystems, Wilmington, MA, USA) and libraries were pooled equimolarly. The final pool was quantified using Qubit, and either 1.3 pM was loaded on a NextSeq 500 instrument (NextSeq 500 HighOutput Kit V2, 150 cycles, Illumina, San Diego, California, United States), with 1–3% PhiX (Illumina), or 0.61-0.65 nM was loaded on a NovaSeq instrument (NovaSeq S1 Reagent kit v1.5, 200 cycles, Illumina) with 1–2% PhiX (Supplemental Table S2). Raw sequencing data is available in the European Genome-Phenome archive (EGAS00001007295).

2.5. Preprocessing and combined mapping of RNA sequencing data

The 'exRNAxeno combined' pipeline was used to preprocess and map the RNA sequencing data (https://github.com/CBIGR/exRNAxeno, accessed on 4 January 2023) [20]. By a combined mapping strategy to the murine and human transcriptome, total RNA sequencing reads are assigned to the right species, either Homo sapiens or Mus musculus. The quality of the data was assessed, and no data points were excluded (Supplemental Table S2). The output of this pipeline is a count table, on which subsequent analyses were performed with RStudio (PBC, version 2022.07.2 Build 576). The MYCN transcription factor target genes used for

our analyses are originating from the Ma'ayan laboratory of computational systems biology (https://maayanlab.cloud/Harmonizome/gene_set/MYCN/CHEA+Transcription+Factor+Targets, accessed on 6 April 2023). The list of neuroblastoma-associated associated mRNAs is derived from a paper of Uemura *et al.* [31]. The percentage of tumoral exRNA is calculated by dividing the number of human reads by the sum of human and murine reads.

2.6. Statistical analysis

Statistical tests were performed by an unblinded researcher with RStudio (PBC, version 2022.07.2 Build 576). The Wilcoxon test, also known as the Wilcoxon rank sum test, was applied to compare group means. This non-parametric test was used as it does not rely on the assumption of a normal distribution, making it suitable for analyzing data with non-normally distributed values. In addition, it is robust to outliers, which is particularly important given the presence of potential extreme values in our dataset. Furthermore, the Wilcoxon test performs well, even with small sample sizes, which is advantageous for our study given the limited number of observations in each group. To explore correlations between random variables, we calculated the Spearman rank correlation coefficient. This test is well-suited for our analysis as it does not assume a linear relationship between variables. In addition, the Spearman rank correlation coefficient is robust to outliers, which is beneficial given the variability observed in our cohorts. Finally, we used the log-rank test to assess differences in survival between groups. This statistical test is commonly used in survival analysis, such as the evaluation of Kaplan-Meier plots. The log-rank test allowed us to determine if there were significant differences in survival outcomes between the groups studied. The pairwise Jaccard similarity coeffient was calculated by counting the number of genes where both samples have transcripts per million (TPM) values greater than 0 and dividing it by the number of genes where at least one sample has a TPM value greater than 0.

3. Results

3.1. The amount of exRNA in blood plasma is driven by tumor size

Mice were subcutaneously engrafted with four different neuroblastoma cell lines: IMR-32, NGP, SK-N-AS and SK-N-BE(2C). A significant correlation between tumor size and exRNA release into the circulation is observed (Spearman correlation = 0.415, $P = 5 \times 10^{-3}$, Figure 1). However, the minimal tumor size for sufficient release of tumoral exRNA (e.g., 1% tumoral exRNA in plasma) depends on the cell line. For instance, IMR-32 reaches more than 1% as soon as tumor size is ~700 mm^3, while other mice need to be sacrificed at higher tumor sizes to be able to reach 1% tumoral exRNA. Furthermore, SK-N-AS tumors are slightly deviating from the observed positive correlation. If the SK-N-AS model is excluded from our analysis, the positive correlation between tumor size and percentage of tumoral exRNA is stronger and more significant (Spearman correlation = 0.554, $P = 7 \times 10^{-4}$, data not shown). Moreover, when considering each cell line separately, a significant trend is not observed, which could be explained by a smaller sample size (reduced power) and by the limited tumor size range

(SK-N-AS: Spearman correlation = 0.515, P = 0.14; SK-N-BE(2C): Spearman correlation = −0.452, P = 0.27; NGP: Spearman correlation = 0.750, P = 0.07; IMR-32: Spearman correlation = 0.442, P = 0.05).

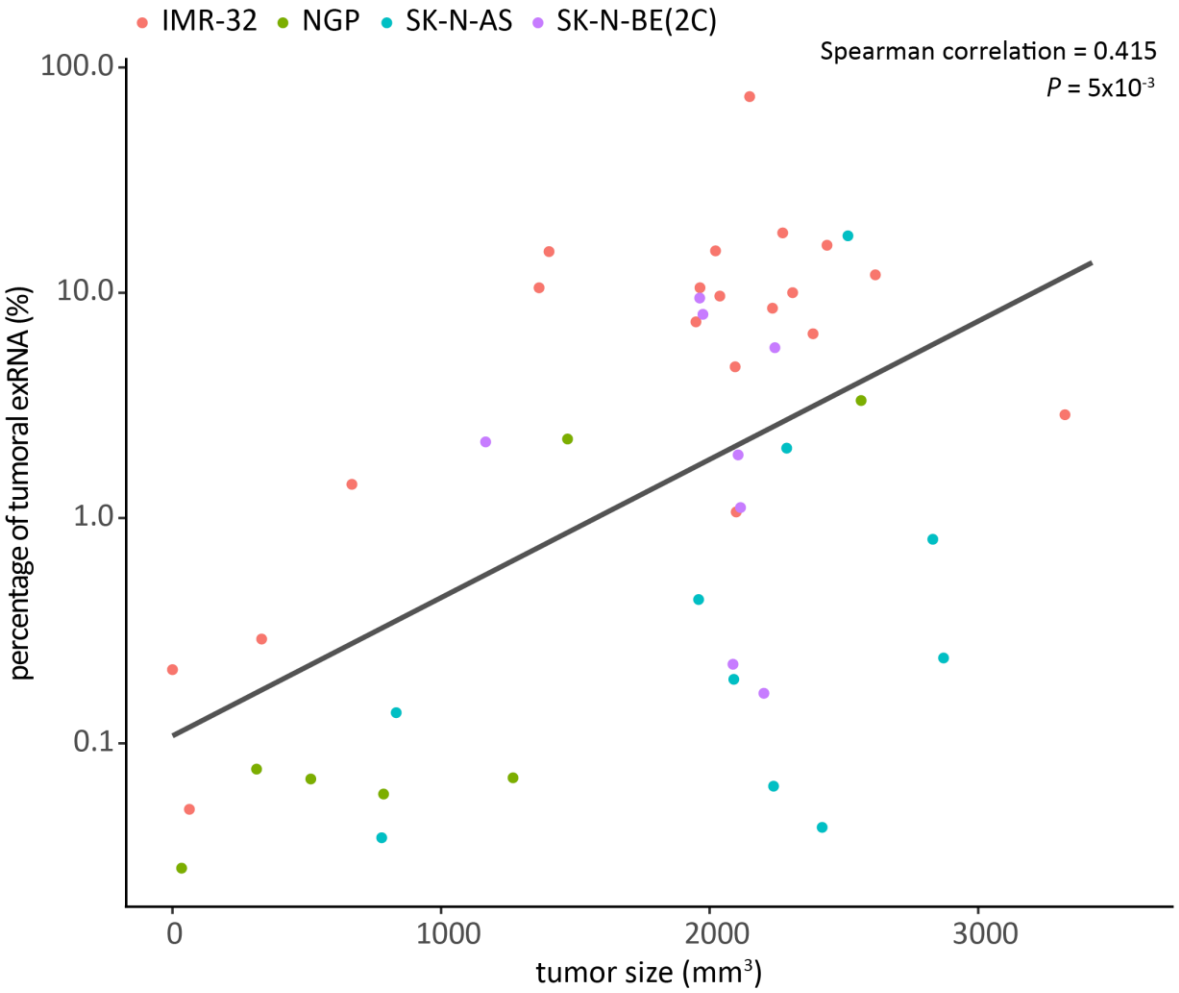

Figure 1. Percentage of tumoral exRNA in function of tumor size in the cell line cohort (n = 45). The different colors represent the different cell-lines. The gray line represents the linear regression line.

3.2. The amount of exRNA in blood plasma is cell line dependent

We demonstrate a high variability in the fraction of tumoral exRNA across different cell lines, with IMR-32 cell line-derived xenografts displaying the highest fraction (Figure 2). Also, a high variability is observed in the number and identity of genes that are detected in mice engrafted with the same cells, even when selecting mice with a tumor size above 1000 mm^3 (Supplemental Figure S1). Also, no commonly detected genes are observed in mice engrafted with different neuroblastoma cell lines (data not shown). Of note, the mouse strain is not associated with the fraction of tumoral exRNA (Supplemental Figure S2).

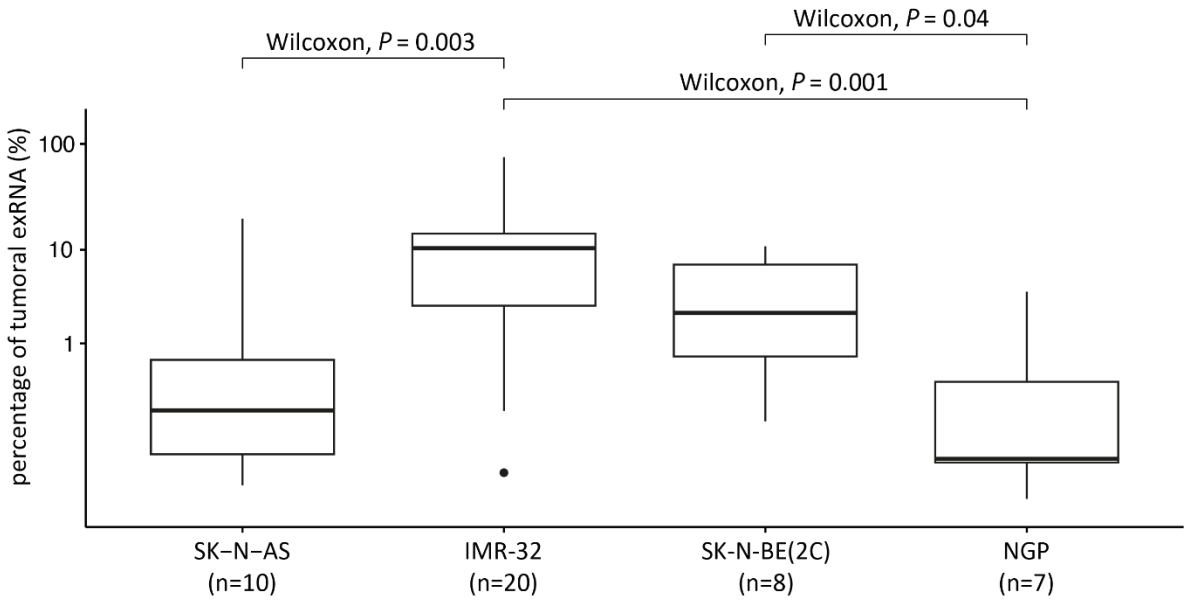

Figure 2. The percentage of tumoral exRNA, grouped per cell line xenograft model. Significant differences between cell lines are indicated with their corresponding Wilcoxon *P* value. The black dot represents an outlier.

3.3. Orthotopic engraftment further increases exRNA levels in IMR-32 model

In a second cohort (*i.e.*, the engraftment site cohort), we studied the potential benefits of orthotopic (intra-adrenal) engraftment compared to heterotopic (subcutaneous) engraftment by selecting the two cell lines with the highest RNA release in the cell line cohort: IMR-32 and SK-N-BE(2C). Subcutaneous engraftment was successful in all mice (IMR-32: n = 10/10, SK-N-BE(2C): n = 10/10). However, three mice dropped out from the orthotopically engrafted group, either during the surgical procedure (IMR-32 engraftment); during follow-up due to an unexpectedly fast deterioration (SK-N-BE(2C) engrafted mouse), or as a consequence of sedation during MRI imaging of an IMR-32 engrafted mouse (IMR-32: n = 8/10, SK-N-BE(2C): n = 9/10). The growth rate of SK-N-BE(2C) tumors is significantly higher than that of IMR-32 tumors, both upon subcutaneous as well as orthotopic engraftment (Supplemental Figure S3).

First, we compared the release between orthotopic and subcutaneous conditions. We found that IMR-32, having a high capacity of releasing tumoral RNA into the circulation from subcutaneous engraftment, releases significantly more exRNA in an orthotopic setting (Figure 3). In some cases, the fraction of human reads reached up to 70%. In contrast, orthotopic SK-N-BE(2C) xenografts do not display higher exRNA levels compared to subcutaneous xenografts (Figure 3).

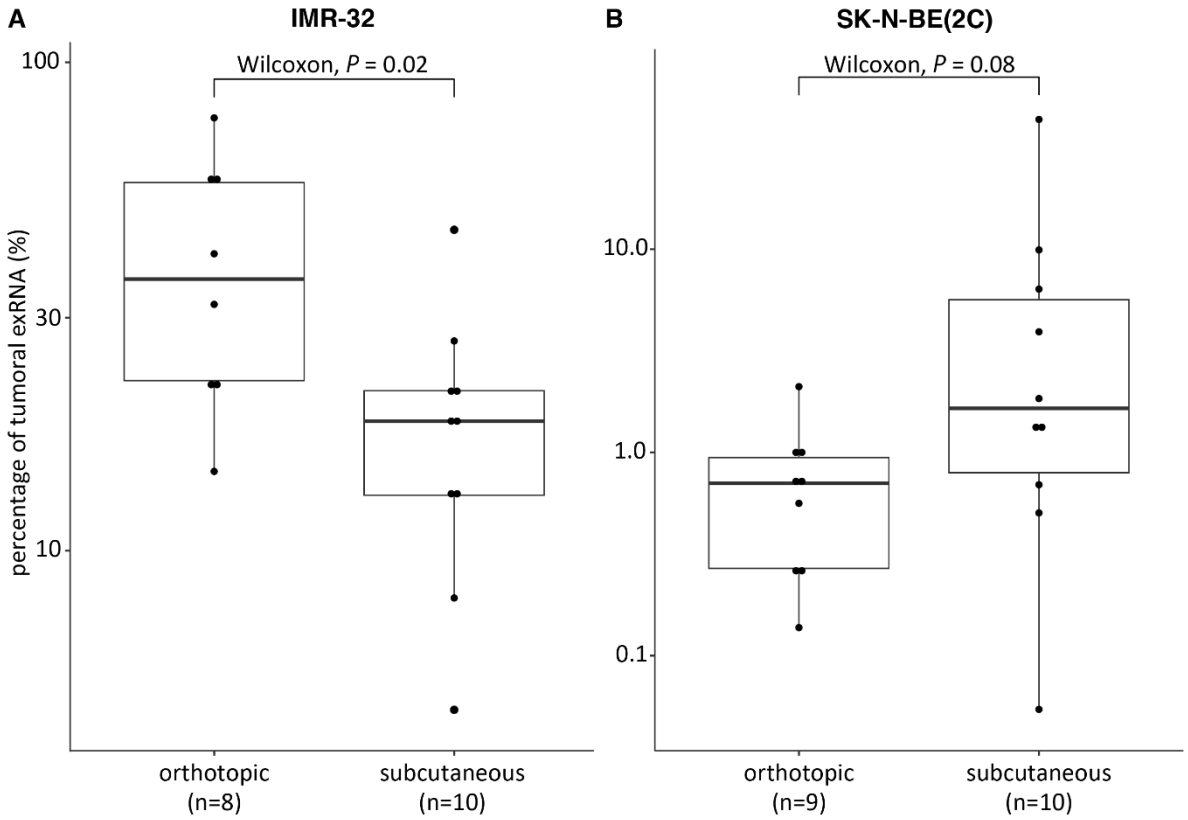

Figure 3. The percentage of tumoral exRNA in mice engrafted orthotopically *versus* subcutaneously with IMR-32 (**A**) or SK-N-BE(2C) (**B**) cells. The black dots represent outliers.

To investigate whether the increased fraction of tumoral circulating RNA leads to improved detectability of relevant genes, we investigated the detectability of a MYCN transcriptional target gene signature (2671 genes) in blood plasma from mice in the engraftment site cohort, which only includes MYCN amplified cell lines. We demonstrate that orthotopic engraftment of IMR-32 significantly increases the percentage of MYCN-associated genes in circulation detected with at least one read, compared to subcutaneous engraftment ($P < 0.001$). More specifically, 48.41–80.04% (median: 65.99%) of MYCN-associated genes are detected orthotopically and 28.75–53.69% (median: 47.83%) are detected subcutaneously (Figure 4A). No significant difference is observed between orthotopic and subcutaneous engraftment of SK-N-BE(2C) cells ($P = 0.55$), *i.e.*, 1.35–16.10% (median: 10.33%) orthotopically *versus* 0.15–39.57% (median: 11.76%) subcutaneously (Figure 4B). In addition to a MYCN transcriptional target gene signature, we also evaluated the detectability of other neuroblastoma-associated genes, and we observed similar patterns (Supplemental Figure S4, [31]).

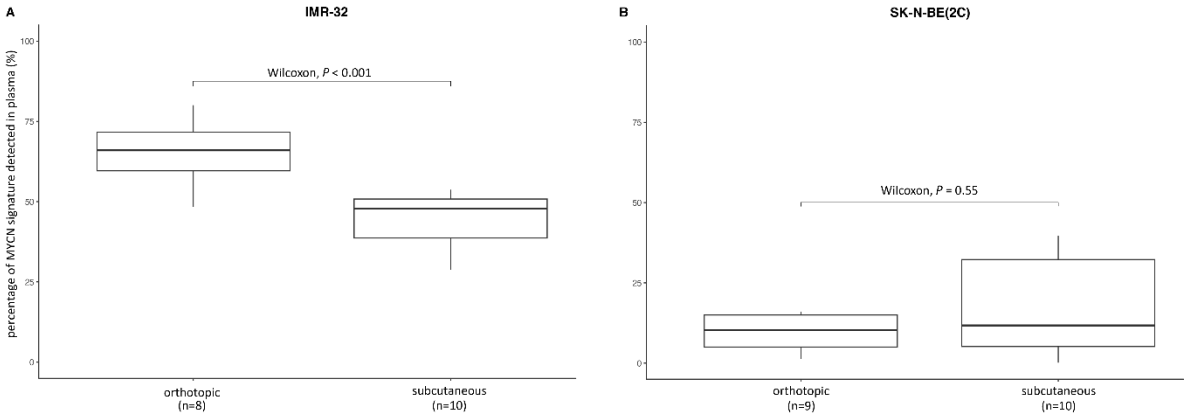

Figure 4. Percentage of MYCN transcriptional target genes, detected in the blood plasma of orthotopically and subcutaneously engrafted mice with IMR-32 (**A**) or SK-N-BE(2C) (**B**) cells.

3.4. Orthotopic engraftment reduces inter-mice variability in tumoral exRNA levels in IMR-32 model

Using the engraftment site cohort, we further evaluate the variability in exRNA transcripts detected across individual mice from a single xenograft model (Supplemental Figure S5). The Jaccard similarity coefficient of detected genes through pairwise comparison of mice in a given model is generally low for each of the xenograft models, confirming a high inter-mice variability (Figure 5). Of note, both IMR-32 xenograft models are less variable compared to the SK-N-BE(2C) models (Wilcoxon $P < 0.001$). Moreover, orthotopic engraftment of IMR-32 cells significantly reduces the variability in tumoral exRNA transcripts detected across individual mice compared to subcutaneous engraftment of the cells (Wilcoxon $P < 0.001$, Figure 5). The variability in murine exRNA transcripts shows the opposite trend in IMR-32 engrafted mice (Supplemental Figure S6). Overall, inter-sample variability is expectedly lower for murine transcripts as compared to human transcripts (Figure 5, Supplemental Figure S6).

In the engraftment site cohort, we further measured tumor growth rate and vascularization to assess potential associations with tumor exRNA amount. Overall, the amount of circulating tumoral RNA is significantly positively correlated with the degree of vascularization (Spearman correlation = 0.84 and $P < 0.001$, Figure 6), while this is not observed for the mitotic count (Spearman correlation = 0.058 and $P = 0.74$, Figure 6). Of note, the overall correlation between exRNA and vascularization was not found when each mouse model was considered separately (SK-N-BE(2C) orthotopic: Spearman correlation = 0.55 and $P = 0.16$, and subcutaneous: Spearman correlation = 0.45 and $P = 0.23$; IMR-32 orthotopic: Spearman correlation = 0 and $P = 1$, and subcutaneous: Spearman correlation = −0.10 and $P = 0.78$). We extended this analysis by performing a histological assessment of the vascularity of subcutaneous SK-N-AS and NGP tumors The significant positive correlation between tumor size and percentage of exRNA remains (Spearman rank correlation = 0.634 and $P < 0.01$, Supplemental Figure S7), but is somewhat less pronounced.

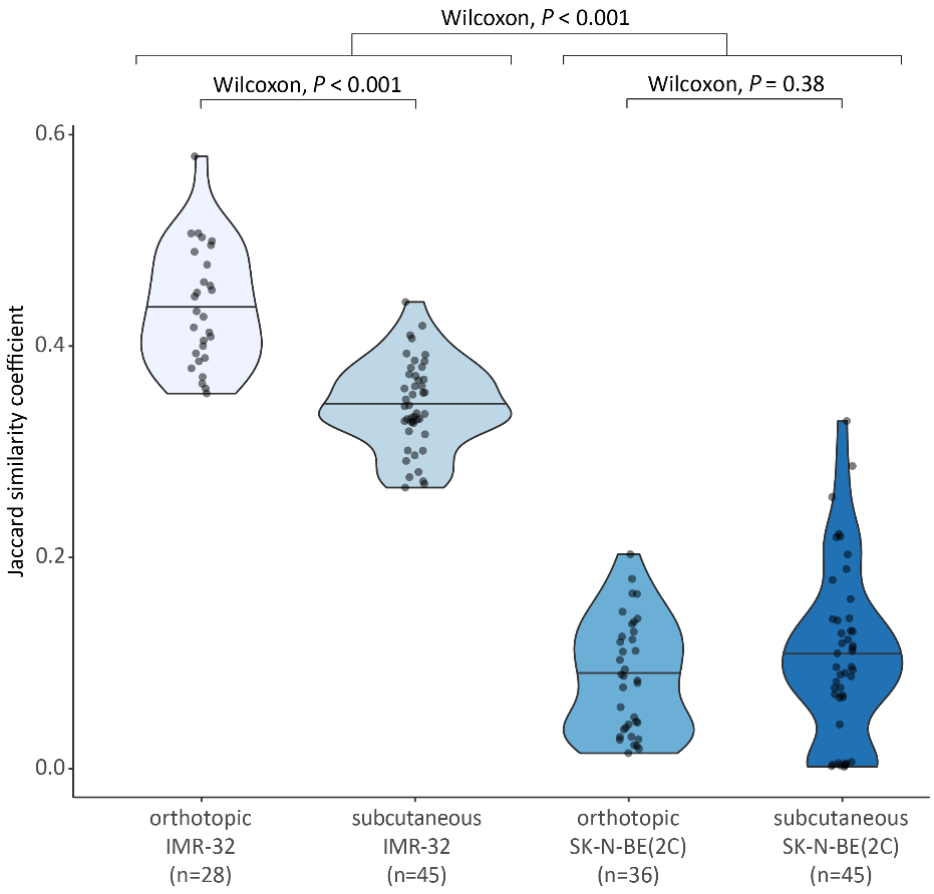

Figure 5. Jaccard similarity coefficient of detected human genes through pairwise comparison of the mice within each model (orthotopic IMR-32, subcutaneous IMR-32, orthotopic SK-N-BE(2C) and subcutaneous SK-N-BE(2C)). The horizontal black line in each model represents the median. IMR-32 and SK-N-BE(2C) tumors display different growth rate and vascularization.

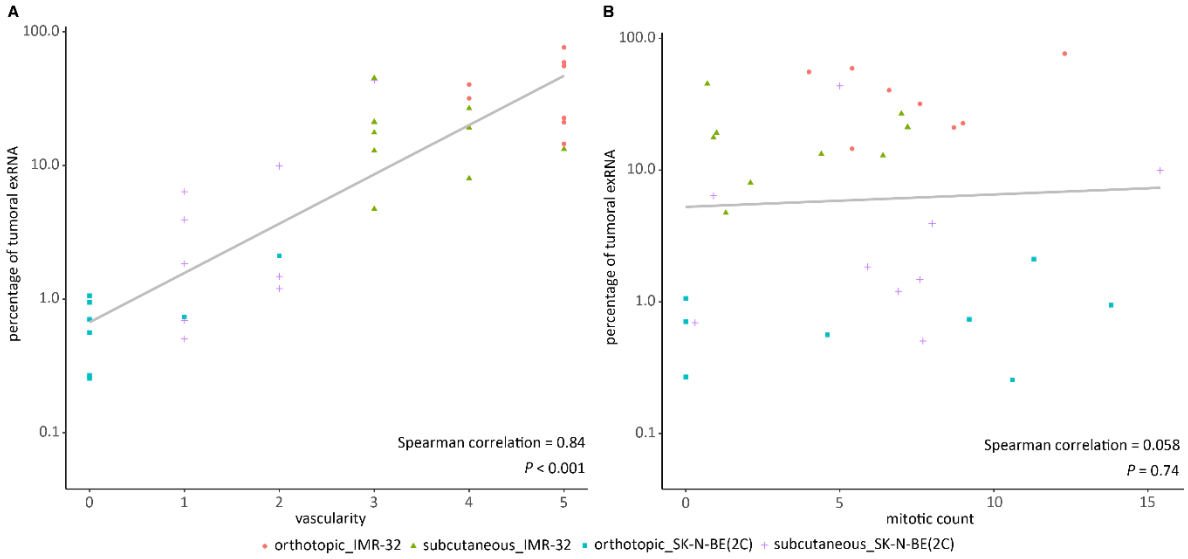

Figure 6. Correlation analysis of the percentage of tumoral exRNA in function of vascularity (**A**) and mitotic count (**B**). The gray line represents the linear regression line. All animals from the engraftment site cohort are included (n = 37).

Based on H&E staining, IMR-32 tumors are significantly more vascularized than SK-N-BE(2C) tumors (Figure 7), which is in line with our macroscopic observation that IMR-32 tumors appear as solid masses, while SK-N-BE(2C) tumors are more fluid and disintegrated (data not shown).

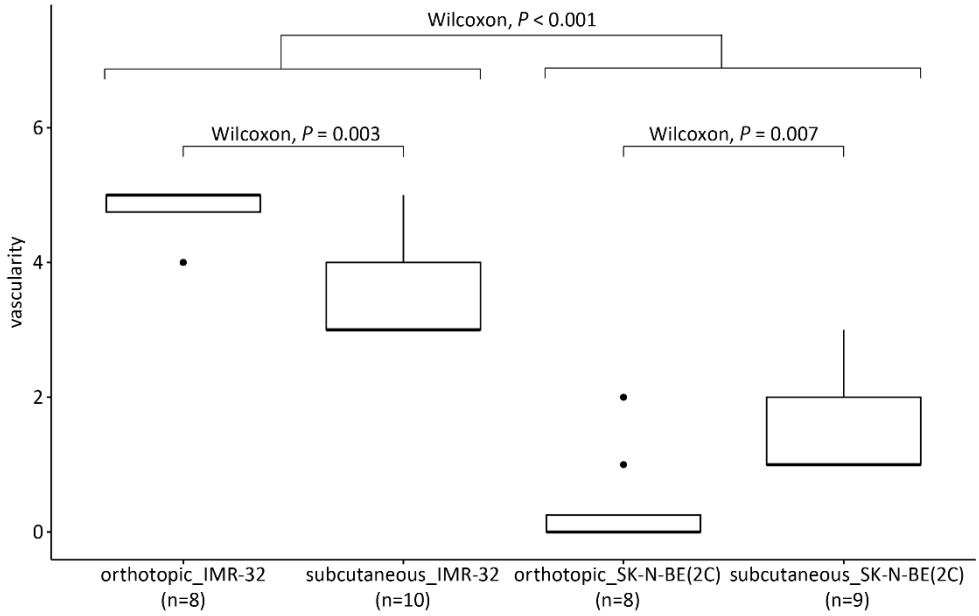

Figure 7. Vascularity levels upon H&E staining of the tumors in the four different models. The black dots represent outliers.

4. Discussion

Accurate assessment of the response to treatment in neuroblastoma patients is highly desired, as half of HR-NB patients experience relapse or refractory disease. Due to its dynamic nature, exRNA is a good analyte to evaluate treatment responses. So far, several studies have been set up, demonstrating the potential of exRNA for detecting and monitoring cancer [32–34]. Due to the limited availability of blood plasma samples from patients participating in clinical trials, and the difficulty in differentiating between normal body and tumor cell-free RNA responses (except for tumor-specific aberrations), we have embarked upon exploring neuroblastoma xenograft models to identify conditions with maximal release of tumoral exRNA into the blood plasma which might be helpful to identify biomarkers. Computational deconvolution of the human and murine sequencing reads from the plasma transcriptome allows the identification of tumor-specific signals.

Mice were engrafted with four different neuroblastoma cell lines: IMR-32, NGP, SK-N-AS and SK-N-BE(2C). A first examination showed a significant correlation between the tumor size and the extent of tumor RNA release into the circulation. The correlation between tumor load and concentration of tumoral cell-free nucleic acids has previously been demonstrated for microRNAs. Zeka *et al.* found 9 miRNAs of which abundance in serum is associated with disease burden and treatment response in children with metastatic neuroblastoma [35]. Further, Van Goethem *et al.* showed that the serum levels of 57 tumoral

miRNAs increase with the tumor size of mice, orthotopically engrafted with a SH-SY5Y neuroblastoma cell line [36]. Now, for the first time, we show similar results for long RNAs such as messenger RNA and long non-coding RNA, jointly called exRNA. Given the assumed higher stability of miRNAs in circulation, this is an important and encouraging finding for future biomarker studies focusing on longer RNA biotypes.

Furthermore, we show that the exRNA levels are dependent on the type of engrafted cells, with IMR-32 being the neuroblastoma cell line with the highest RNA release into the blood circulation in both study cohorts. The observed differences among models is consistent with our previous finding that the fraction of tumoral exRNA varies widely among engrafted tumor entities (both pediatric and adult cancers, *i.e.*, melanoma, penile, endometrial, breast and lung cancer) [20]. When examined at the macroscopic level, tumors display a varied composition across different cell lines. Some tumors consist of solid masses (e.g., IMR-32), while others are more hemorrhagic and disintegrate during the process of tumor resection (e.g., SK-N-BE(2C)). Through microscopic analysis of H&E stained tumor tissue, IMR-32 engrafted tumors are more vascularized than SK-N-BE(2C) tumors. This may underly the observation of higher levels of tumoral exRNA in the plasma of IMR-32 engrafted mice. This hypothesis is further supported by a significant positive correlation between vascularity and the fraction of tumoral exRNA in the plasma.

The SK-N-AS engrafted mice are slightly deviating from the observed correlation. More specifically, for a given tumor size or vascularity score, the percentage of exRNA is variable. This suggests that also other characteristics of the engrafted cells not studied here, such as metastatic potential, genetic profile, origin of neuroblastoma cell lines (abdominal, bone *etc.*), or release potential of extracellular vesicles may contribute to the observed exRNA differences. Unfortunately, in our study, the extent of metastatic disease was not assessed since follow-up of the orthotopic xenografts was done using MRI, focusing only on the left adrenal gland, and no organs were collected. Moreover, the amount of cell lines included was too sparse to define a correlation with the genetic background or origin of neuroblastoma cell lines. Furthermore, it remains to be determined whether treatment would alter the quantities of tumoral exRNA.

When looking deeper into the differences between orthotopic and subcutaneous engraftment, we observe that orthotopic IMR-32 grafts have significantly higher levels of vascularization, possibly contributing to higher levels of tumor exRNA in the plasma. Intriguingly, for SK-N-BE(2C), orthotopic engraftment is associated with reduced vascularity and less tumoral exRNA in the plasma. This might be caused by the aggressive nature of SK-N-BE(2C), which is a very rapidly growing cell line *in vivo*. The short duration of SK-N-BE(2C) tumor growth might be insufficient for the development of blood vessels and the entry of tumoral RNA into circulation. Orthotopic engraftment of the SK-N-BE(2C) cells further enhanced the tumor growth rate as compared to subcutaneous engraftment of SK-N-BE(2C), which may also explain why the fraction of tumoral exRNA and the amount of blood vessels are further reduced in this orthotopic setting. Neo-angiogenesis in adrenal tumors has previously been shown to occur at day 15, while the orthotopic SK-N-BE(2C) mice in our study were sacrificed between 10 and 17 days after engraftment [37]. Of note,

other tumor characteristics, such as necrosis have been studied as well, for instance demonstrating that the extent of necrosis of lung adenocarcinoma positively correlates with the amount of tumoral extracellular DNA that can be detected in blood plasma [38]. Clearly, tumor characteristics may play a role, even in the absence of immunosurveillance.

Another important finding is the high variability in number of detectable tumor transcripts among mice engrafted with different cells, but also within one model. This is remarkable since mice from the same model are being engrafted with cells originating from the same homogeneous cell suspension. This high variability in detected tumor transcripts makes biomarker discovery challenging. To address this, we evaluated whether orthotopic engraftment of two different cell lines reduces the inter-mice variability within a single model. We demonstrate that this is indeed the case for IMR-32 when considering tumoral exRNA. The murine exRNA shows the opposite trend in IMR-32 engrafted cells, likely because of the compositional nature of sequencing data as a finite number of reads are generated during a sequencing run. If the proportion of human-derived reads increases, fewer reads will represent murine exRNA. The exRNA transcript variability within the IMR-32 engrafted mice is in general significantly lower than the variability detected in the SK-N-BE(2C) model. Furthermore, orthotopic engraftment instead of subcutaneous engraftment of IMR-32 cells, causes the fraction of human reads to increase significantly. The reduced variability in the (orthotopic) IMR-32 model might be attributed to the higher tumoral exRNA fraction that is observed in all mice of this model.

In future studies, it might be valuable to study the effect of metastatic disease on exRNA levels. For ctDNA, it has been reported that metastatic lesions are associated with a higher ctDNA fraction in the circulation of patients with neuroblastoma or adult cancers, such as breast cancer [8,14,16,39]. Also, evaluating another animal model, such as a xenografted rat, may provide additional insights into the biomarker potential of liquid biopsies of xenografts. A rat contains about 10 times more blood than a mouse, enabling an investigator to collect weekly volumes of ~1.4 ml, allowing to study how the tumoral exRNA quantity and dynamics change during disease progression or treatment.

5. Conclusion

In conclusion, the type of cell line, its site of engraftment and tumor size are factors that contribute to the amount of circulating tumoral RNA and should therefore carefully be considered when performing experiments studying and exploiting circulating RNA biomarkers.

Supplementary Data

The authors confirm that the supplementary data are available within this article. Figure S1: The overlap of genes between the mice engrafted with IMR-32 (A; n = 16), NGP (B; n = 3), SK-N-AS (C; n = 8) or SK-N-BE(2C) (D; n = 8); Figure S2: Percentage of tumoral exRNA in the different engrafted mouse strains; Figure S3: Kaplan-Meier curve depicting the probability of survival in function of the lifespan (days) for four different mouse cohorts: subcutaneously engrafted mice with either IMR-32 or SK-N-BE(2C) cells (A) and orthotopically engrafted mice with either IMR-32 or SK-N-BE(2C) cells (B); Figure S4:

Percentage of neuroblastoma associated genes, detected in the blood plasma of orthotopically and subcutaneously engrafted mice with IMR-32 (A) or SK-N-BE(2C) (B) cells; Figure S5: Gene overlap in orthotopically (A: n = 9) and subcutaneously (B: n = 10) engrafted SK-N-BE(2C) xenografts, and orthotopically (C: n = 8) and subcutaneously (D: n = 10) engrafted IMR-32 xenografts; Figure S6: Jaccard similarity coefficient obtained by pairwise comparison of murine gene counts (transcripts per million) of the samples within each model (orthotopic IMR-32, subcutaneous IMR-32, orthotopic SK-N-BE(2C) and subcutaneous SK-N-BE(2C)); Figure S7: Correlation analysis of the percentage of tumoral exRNA in function of vascularity; Table S1: Characteristics and genetic background of the cell lines that were engrafted in the mice included in our study [40–42]; Table S2: Overall, the sequencing data is of good quality. For each RNA sample (RNA ID), the matching mouse ID, biomaterial ID, sample type, mouse cohort, tumor size, plasma input volume and added spike concentrations are shown, as well as haemolysis levels measured by NanoDrop technology (absorbance of light at 414 nm) and RNA sequencing QC results.

Acknowledgments

We thank Benedicte Descamps and Christian Vanhove from the INFINITY imaging core at Ghent University for their assistance in performing the MRI scans on the mice and for their help in interpreting the obtained images. We would also like to acknowledge that part of the results of this research was presented as a poster entitled ‘Exploration of neuroblastoma xenograft models for the analysis of tumoral cell-free RNA in murine blood plasma’ at the ANR (Advances in Neuroblastoma Research association) meeting held in Amsterdam in May 2023. Funding: This work was supported by Kom op tegen Kanker (Stand up to Cancer, the Flemish cancer society, granted to BDW, JV and TVM, 2022/13037 to KS); the Ghent University Special Research Fund (BOF22/CDV/077 to JD and BDW, 202011/GE/ZAP/018 to KD); the Research Foundation – Flanders (G0B2820N to JV, LIQUIDHOPE TRANSCAN-2 project to JV, 1224021N to AD, senior clinical researcher grant to BDW, 1S90621N to JDW, 11M1422N to MR) and the “Geconcerteerde onderzoeksactie” (GOA), Ghent University: Replication fork protector dependency factors as novel targets for combination treatment and immunomodulation in neuroblastoma (BOF22/GOA/009 to FS, BDW, JV, JD and HVD).

Conflicts of Interests

The authors have no conflicts of interest to declare.

Ethical Statement

The authors are accountable for all aspects of the work in ensuring that questions related to the accuracy or integrity of any part of the work are appropriately investigated and resolved. Experiments were performed under a project license (NO.: P164/2019, ECD 18-58, ECD 18-74, ECD 20-55 and ECD 20-63) granted by institutional ethics committees of KU Leuven and UGent in compliance with the universities’ (KU Leuven and UGent) national or institutional guidelines for the care and use of animals.

Authors’ Contribution

Conception and design: B.D.W., H.V.D., J.D., J.V. and T.V.M.; Administrative support: B.D.W., J.V. and T.V.M.; Provision of study materials and patients: H.V.D., J.D., J.D.W.,

J.N., K.S., K.V., L.M., M.R., M.V.T. and N.Y.; Collection and assembly of data: H.V.D. and J.D.; Data analysis and interpretation: H.V.D. and J.D.; Writing – Original Draft: all authors; Writing—review and editing: all authors. All authors have read and agreed to the published version of the manuscript.

References

1. Johnsen JI, Dyberg C, Wickström M. Neuroblastoma—A neural crest derived embryonal malignancy. *Front. Mol. Neurosci.* 2019, 12:9.
2. Gomez RL, Ibragimova S, Ramachandran R, Philpott R, Ali FR. Tumoral heterogeneity in neuroblastoma. *Biochim. Biophys. Acta Rev. Cancer* 2022, 1877:188805.
3. DuBois SG, Macy ME, Henderson TO. High-Risk and Relapsed Neuroblastoma: Toward More Cures and Better Outcomes. *Am. Society Clin. Oncol. Educ. Book* 2022, 42: 768–780.
4. Pasqualini C, Valteau-Couanet D, Ladenstein R. High-risk neuroblastoma standard clinical practice recommendations. Available: https://www.srohp.ro/wp-content/uploads/2022/01/escp-high-risk-neuroblastoma-standard-clinical-practice-recommendations.pdf.
5. Pinzani P, D'Argenio V, Del Re M, Pellegrini C, Cucchiara F, *et al.* Updates on liquid biopsy: Current trends and future perspectives for clinical application in solid tumors. *Clin. Chem. Lab. Med.* 2021, 59(7):1181–1200.
6. Schmelz K, Toedling J, Huska M, Cwikla MC, Kruetzfeldt LM, *et al.* Spatial and temporal intratumour heterogeneity has potential consequences for single biopsy-based neuroblastoma treatment decisions. *Nat. Commun.* 2021, 12:6804.
7. Chicard M, Colmet-Daage L, Clement N, Danzon A, Bohec M, *et al.* Whole-exome sequencing of cell-free DNA reveals temporo-spatial heterogeneity and identifies treatment-resistant clones in neuroblastoma. *Clin. Cancer Res.* 2018, 24(4):939–949.
8. Lodrini M, Graef J, Thole-Kliesch TM, Astrahantseff K, Sprüssel A, *et al.* Targeted Analysis of Cell-free Circulating Tumor DNA is Suitable for Early Relapse and Actionable Target Detection in Patients with Neuroblastoma. *Clin. Cancer Res.* 2022, 28(9):1809–1820.
9. Cimmino F, Lasorsa VA, Vetrella S, Iolascon A, Capasso M. A Targeted Gene Panel for Circulating Tumor DNA Sequencing in Neuroblastoma. *Front. Oncol.* 2020, 10:596191.
10. Combaret V, Iacono I, Bellini A, Brégon S, Bernard V, *et al.* Detection of tumor ALK status in neuroblastoma patients using peripheral blood. *Cancer Med.* 2015, 4:540–550.
11. Lodrini M, Sprüssel A, Astrahantseff K, Tiburtius D, Konschak R, *et al.* Using droplet digital PCR to analyze MYCN and ALK copy number in plasma from patients with neuroblastoma. *Oncotarget* 2017, 8(49):85234–85251.
12. Peitz C, Sprüssel A, Linke RB, Astrahantseff K, Grimaldi M, *et al.* Multiplexed Quantification of Four Neuroblastoma DNA Targets in a Single Droplet Digital PCR Reaction. *J. Mol. Diagn.* 2020, 22(11):1309–1323.
13. Kahana-Edwin S, Cain LE, McCowage G, Darmanian A, Wright D, *et al.* Neuroblastoma molecular risk-stratification of DNA copy number and ALK genotyping via cell-free circulating tumor DNA profiling. *Cancers* 2021, 13(3):3365.
14. Van Roy N, Van Der Linden M, Menten B, Dheedene A, Vandeputte C, *et al.* Shallow whole genome sequencing on circulating cell-free DNA allows reliable noninvasive copy-number profiling in neuroblastoma patients. *Clin. Cancer Res.* 2017, 23(20):6305–6315.
15. Bosse KR, Giudice AM, Lane MV, McIntyre B, Schürch, PM, *et al.* Serial profiling of circulating tumor DNA identifies dynamic evolution of clinically actionable genomic alterations in high-risk neuroblastoma. *Cancer Discov*. 2022,12(12):2800–2819.

16. Chicard M, Boyault S, Daage LC, Richer W, Gentien D, *et al.* Genomic copy number profiling using circulating free tumor DNA highlights heterogeneity in neuroblastoma. *Clin. Cancer Res.* 2016, 22(22):5564–5573.
17. Cao M. The extracellular RNA and drug resistance in cancer: a narrative review. *ExRNA* 2023,5:1.
18. Ni Y, Zhang W, Mu G, Gu Y, Wang H, *et al.* Extracellular RNA profiles in non-small cell lung cancer plasma. *J. Thorac. Dis.* 2023, 15(5):2742–2753.
19. Li Z, Gao Y, Cao Y, He, F, Jiang R, *et al.* Extracellular RNA in melanoma: Advances, challenges, and opportunities. *Front. Cell. Dev. Biol.* 2023, 11:1141543.
20. Vermeirssen V, Deleu J, Morlion A, Everaert C, De Wilde J, *et al.* Whole transcriptome profiling of liquid biopsies from tumour xenografted mouse models enables specific monitoring of tumour-derived extracellular RNA. *NAR Cancer* 2022, 4(4):zcac037.
21. Wang Y, Cui J, Wang L. Patient-derived xenografts: a valuable platform for clinical and preclinical research in pancreatic cancer. *Chin. Clin. Oncol*. 2019, 8(2):17.
22. Harenza JL, Diamond MA, Adams RN, Song MM, Davidson HL, *et al.* Transcriptomic profiling of 39 commonly-used neuroblastoma cell lines. *Sci. Data* 2017, 4:170033.
23. Van Goethem A, Yigit N, Moreno-Smith M, Vasudevan SA, Barbieri E, *et al.* Dual targeting of MDM2 and BCL2 as a therapeutic strategy in neuroblastoma. *Oncotarget* 2017, 8(34):57047–57057.
24. Rihani A, Van Goethem A, Ongenaert M, De Brouwer S, Volders PJ, *et al.* Genome wide expression profiling of p53 regulated miRNAs in neuroblastoma. *Sci. Rep.* 2015, 5(1):9027.
25. Neuberg D. How many mice? Design considerations for murine studies. *Blood Adv.* 2017, 1:1466.
26. Takahashi A. Toward Understanding the Sex Differences in the Biological Mechanism of Social Stress in Mouse Models. *Front. Psychiatry* 2021, 12:644161.
27. Bielohuby M, Herbach N, Wanke R, Maser-Gluth C, Beuschlein F, *et al.* Growth analysis of the mouse adrenal gland from weaning to adulthood: time- and gender-dependent alterations of cell size and number in the cortical compartment. *Am. J. Physiol. Endocrinol. Metab.* 2007, 293(1):139–146.
28. Deveson IW, Chen WY, Wong T, Hardwick SA, Andersen SB. *et al.* Representing genetic variation with synthetic DNA standards. *Nat Methods* 2016, 13(9):784–791.
29. Hulstaert E, Decock A, Morlion A, Everaert C, Verniers K, *et al.* Messenger RNA capture sequencing of extracellular RNA from human biofluids using a comprehensive set of spike-in controls. *STAR Protoc.* 2021, 2(2):100475.
30. Everaert C, Helsmoortel H, Decock A, Hulstaert E, Van Paemel R, *et al.* Performance assessment of total RNA sequencing of human biofluids and extracellular vesicles. *Sci. Rep.* 2019, 9(1):17574.
31. Uemura S, Ishida T, Thwin KKM, Yamamoto N, Tamura A, *et al.* Dynamics of Minimal Residual Disease in Neuroblastoma Patients. *Front. Oncol.* 2019, 9:455.
32. Krug AK, Enderle D, Karlovich C, Priewasser T, Bentink S, *et al.* Improved EGFR mutation detection using combined exosomal RNA and circulating tumor DNA in NSCLC patient plasma. *Ann. Oncol.* 2018, 29:700–706.
33. Larson MH, Pan W, Kim HJ, Mauntz RE, Stuart SM, *et al.* A comprehensive characterization of the cell-free transcriptome reveals tissue- and subtype-specific biomarkers for cancer detection. *Nat Commun.* 2021, 12: 2357.
34. Happel C, Ganguly A, Tagle DA. Extracellular RNAs as potential biomarkers for cancer. *J. Cancer Metastasis Treat.* 2020, 6:32.
35. Zeka F, Van Goethem A, Vanderheyden K, Demuynck F, Lammens T, *et al.* Circulating microRNA biomarkers for metastatic disease in neuroblastoma patients. *JCI Insight* 2018, 3(23):e97021.

36. Van Goethem A, Deleu J, Yigit N, Everaert C, Moreno-Smith M, *et al.* Longitudinal evaluation of serum microRNAs as biomarkers for neuroblastoma burden and therapeutic p53 reactivation. *NAR Cancer* 2023, 5:zcad002.
37. Daudigeos-Dubus E, LE Dret L, Rouffiac V, Bawa O, Leguerney I, *et al.* Establishment and characterization of new orthotopic and metastatic neuroblastoma models. *In Vivo* 2014, 28(4):425–434.
38. Karasaki T, Moore DA, Veeriah S, Naceur-Lombardelli C, Toncheva A, *et al.* Evolutionary characterization of lung adenocarcinoma morphology in TRACERx. *Nat. Med.* 2023, 29:833–845.
39. Bera A, Russ E, Karaian J, Landa A, Radhakrishnan S, *et al.* Circulating Cell-free DNA in Serum as a Marker for the Early Detection of Tumor Recurrence in Breast Cancer Patients. *Cancer Diagn. Progn.* 2022, 2(3):285–292.
40. Linder S, Bachmann HS, Odersky A, Schaefers S, Klein-hitpass L, et al. Absence of telomerase reverse transcriptase promoter mutations in neuroblastoma. *Biomed. Rep.* 2015, 3(4):443–446.
41. Chen L, Rousseau RF, Middleton SA, Nichols GL, Newell DR, *et al*. Pre-clinical evaluation of the MDM2-p53 antagonist RG7388 alone and in combination with chemotherapy in neuroblastoma. *Oncotarget* 2015, 6(12):10207–10221.
42. Thiele CJ. Neuroblastoma Cell Lines. *J. Human Cell Culture* 1998, 1:21–53.